ACIS Memo #_____

Massachusetts Institute of Technology
Center For Space Research
Cambridge, Massachusetts 02139

Room 37-662C, e-mail: sjones@space.mit.edu

From: Stephen Jones
To: ACIS Team
Subject: HEXS Flat Field Pileup Analysis - Work in Progress
Date: August 2, 1997

1 Introduction

In the low flux limit x-rays incident on a CCD are assumed to be independently detectable. That is, the detection of any x-ray is not affected by the presence of any other x-rays. At higher flux this approximation breaks down as "pileup" occurs. Note that the piled-up x-rays are not directly interacting with each other, but that the pattern of their electron charge clouds, which form in the depleted region of the CCD, are merging or even overlapping. All single x-rays produce charge clouds whose detection pattern varies strongly with (1) the x-ray energy, (2) the sub-pixel location of the initial photoelectric interaction, (3) the depth of the interaction, and (4) the detector electronics. All detections, or events, can be catagorized by (1) the shape (grade) and (2) the magnitude (energy) of their charge cloud pattern. Figure 1 represents a matrix of the possible grade-energy combinations for which a single x-ray can be detected. The x-ray counts for a timed exposure will divide amoung the catagories. In the low flux limit, the probability of a single x-ray to land in any catagory is proportional to the relative ratio of counts in the four catagories. These branching ratios will be specific to the x-ray source and the detector's characteristics. However, the branching ratios are not independent of the incident flux, and their variation with flux is the essential problem of pileup. The effect of pileup is to redistribute the counts in each catagory, as exemplified by the arrows in the figure.

The largest effect of merging charge clouds is to reduce the number of detected good x-rays. The merged cloud will most likely be detected as a single x-ray with either a different grade (e.g. if the two x-rays landed in adjacent pixels) or a different energy (e.g. if the two x-rays landed in the same pixel). Many cases will appear as mixtures of these types of pileup. In either case, as a second good x-ray lands near a first good x-ray, not only is the second x-ray undetected, but the first x-ray is removed from detection as a good event. These major redistributions are represented by the heavy arrows in Fig. 1. The smaller redistributions shown by the light arrows occur very infrequently for quasi-monochromatic x-ray beams and are not considered here.

There are two complications in a general pileup analysis. The first is spatial uniformity of the incident flux. If the effect of an x-ray event with the depleted silicon layer was always contained within one pixel, then event detection for any pixel is independent of all other pixels and pileup effects only occur when two x-rays land in the same pixel. Thus, gradients in the incident flux do

not alter independent pileup effects. However, this is not the general behavior of the ACIS CCDs in which several pixels can respond to a single x-ray. Since the basis for this paper is experimental data with uniform illumination, we focus our analysis on that regime. A short section at the end of this paper discusses pileup in the single pixel limit.

The second complication for pileup analysis is the spectral shape of the incident flux. Here there are two limits, a monochromatic source and a continuum source. The strategy followed in this paper is to examine a monochromatic source first to understand the redistribution of x-rays at each energy. Then, an approximation technique will be discussed to apply these results to any spectral shape, including a coninuum source.

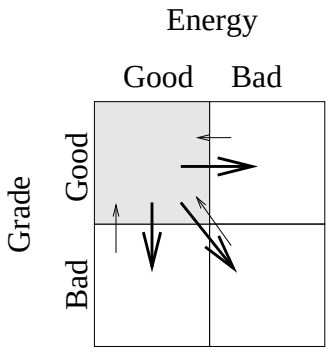

Figure 1: Possible redistributions of detected x-rays due to pileup

2 Model

We start by defining any detected x-ray with the desired energy and grade to be "good"; all others are defined as "bad". Since the incident x-ray beam is not purely monochromatic, but typically has a mixture of a monochromatic line with other spectral features, in the low flux, or non-pileup limit for every "good" x-ray there are α "bad" x-rays. If the incident flux of good x-rays is N_i x-rays per exposure per CCD, then the total flux of all detected x-rays is $(1+\alpha)$. This quasi-monochromatic combined beam is a good representation of the x-ray sources used in the ACIS quantum efficiency calibration.

Although each exposure is the accumulation of N_i incident x-rays, for the purposes of analysis we can picture the x-rays as striking the CCD serially instead of simultaneously. The goal is to describe a function $N_d(N_i)$ which represents the number of detected good x-rays as a function of the number of incident good x-rays. Then by taking the inverse of this function, N_i can be determined from an experimental measurement of N_d. We begin construction of this function by examining the effect of a single x-ray.

Let ϵ be the effective area of the CCD affected by absorption of a "good" x-ray (typically the desired energy is a k_α x-ray and the desired shape are ASCA grades 0,2,3,4,and 6). In general, $\epsilon = \epsilon(E)$ will be a functuon of energy. Similarly, $\epsilon^{'}$ is the average effective area corresponding to all other x-rays, i.e. those with different energies and grades. The physical meaning of ϵ is that if

a second x-ray lands near a prior x-ray such that the center of the second photoelectric absorption occurs within the area ϵ of the first x-ray, then an interaction occurs. Specific interaction effects are described mathematically below. Since a pixel's response to an x-ray is all or nothing (that is, there is no subpixel resolution) we can derive the minimum size for ϵ commesurate with our event detection criteria. All event discrimination is based on the 3x3 pixel subarray surrounding a local maximum of detected charge. Thus, any second x-ray landing within the subarray invokes an interaction, and the area of 9 pixels forms a lower limit for ϵ. Nine pixels corresponds to a fractional area of 3.4×10^{-5} for one quadrant of a CCD17.

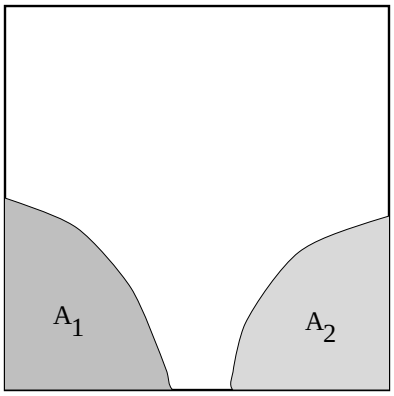

Figure 2: Regions of CCD for pileup model

The mathematical model begins by schematically dividing the area of CCD as shown in Fig. 2. Assuming the total surface area of the CCD is normalized to 1, let A_1 be the total area occupied by all good x-rays. The number of detected events is taken to be $N_d = A_1/\epsilon$. This assumption is approximate since two good x-rays could lie close enough together so that their ϵs overlap while they do not interact. Let A_2 be the total area occupied by all other x-rays. Then $1 - A_1 - A_2$ is the CCD area unblemished by any x-ray. The probablity for an incident x-ray to land on a previous good x-ray is A_1, the probablity for an incident x-ray to land on a previous bad x-ray is A_2, and the probablity for an incident x-ray to land in unperturbed pixels and be solely detected is $1 - A_1 - A_2$. The effect of an incident x-ray landing in A_1 is removal of one previous x-ray from A_1 while adding some area ϵ'' to A_2, which must be between 1 and 2 times ϵ. We assume than any x-ray landing in A_2 does not change either A_1 or A_2. Finally, we assume that A_1 can increase only by good photons landing in $1 - A_1 - A_2$. Then the variation of A_1 and A_2 with N_i can be described by the following pair of ordinary differential equations:

$$\frac{dA_1}{dN_i} = (1 - A_1 - A_2)\epsilon - A_1\epsilon(1 + \alpha) \tag{1}$$

$$\frac{dA_2}{dN_i} = (1 - A_1 - A_2)\alpha\epsilon^{'} + A_1\epsilon^{''}(1+\alpha) \tag{2}$$

The solution is obtained by combining the two equations to separate variables. This results in a second order differential equation with the following solution,

$$A_1 = \epsilon/\beta exp(-\hat{\epsilon}N_i)sin(\beta N_i) \tag{3}$$

where

$$\hat{\epsilon} = \epsilon(1 + \alpha/2(1 + \epsilon^{'}/\epsilon), \tag{4}$$
$$\beta = \sqrt{(1+\alpha)(\alpha\epsilon\epsilon^{'} + \epsilon\epsilon^{''}) - \epsilon^2\hat{\epsilon}^2}$$

Using $A_1 = \epsilon N_d$, this formula has the desired asymtotic limit of $N_i = N_d$ for low flux, with the following expansion for the logrithm of the ratio:

$$log(\frac{N_d}{N_i}) = log(c) - \hat{\epsilon}N_i - \beta^2 N_i^2/6) \tag{5}$$

In the limit where $\epsilon \sim \epsilon^{'}$ then
$\beta = \epsilon\sqrt{(\epsilon^{''}/\epsilon - 1)(1+\alpha)}$

For fluxes that are not high enough to invoke the quadratic term of Eqn. 5, N_i can be determined from N_d if $\hat{\epsilon}$ is known. The three variable are related by the transendental equation

$$N_d = N_i exp(-\hat{\epsilon}N_i) \tag{6}$$

Solutions to Eqn. 6 are plotted in Fig. 3 for two different flux ranges and for $\hat{\epsilon}$=0,2,4,...50 (x10^5). Specifically, the cross-section $\hat{\epsilon}$ equals the fractional area of a CCD region of interest, and N_d and N_i are the corresponding counts in that region. As an example, the ACIS calibration frequently analysis data within a quadrant of a CCD-17, or a region of 256x1024 pixels. Thus, $\hat{\epsilon} = 10 \times 10^{-5}$ corresponds to a area of 26.2 pixels. The deviation from the line $N_i = N_d$ increases as $\hat{\epsilon}$ increases. Also, the curve bends over for significantly high pileup. this corresponds to the condition where so many charge clouds overlap that very few satisfy the event selection criteria. All curves for $\hat{\epsilon} > 0$ should assymtote to 0 for high enough N_i.

3 Experiment

The experimental technique to measure ϵ and $\hat{\epsilon}$ used the High Energy X-ray Source (HEXS) at MIT's CCD Calibration Facility. HEXS is the same source used for the ACIS quantum efficiency calibration, so careful measurements of pileup using that source are particularly important for the AXAF program. The HEXS source uses fluorescence from 12 different targets ranging from Al to Ge as shown in Table 1. The fluorescence spectrum is generated by the bremsstrahlung spectrum from a commercial electron impact x-ray tube using a Mo target. The tube current and voltage

are independently adjustable and are temporally stable to within a percent. The maximum tube power is 9 W, with a maximum voltage of 30 kV.

Table 1. HEXS targets, energies, and x-ray penetration length in silicon

Target	Energy	X-ray mfp in Si
	(eV)	μm
Al	1487	8.0
Si	1740	12.4
P	2015	1.6
Cl	2622	3.1
Ti	4508	13.6
V	4949	17.7
Fe	6399	36.9
Co	6925	46.4
Ni	7471	57.8
Cu	8040	71.6
Zn	8630	88.0
Ge	9874	130.7

All detectors used for this analysis are CCDID-17s, produced by Lincoln Labs, which have a 1024x1024 array of 24 μm square pixels. As mentioned above, each CCD is divided into 4 readout quadrants of 256x1024 pixels. Since the gain from each quadrant can be different, most analysis is conducted on a quadrant basis rather than on the entire CCD. Each CCD was flight qualified for ACIS although only w140c4r was selected for the flight focal plane.

A series of 11 pileup measurements were conducted using either different CCDs, different HEXS configurations, different electronics and different exposure times. The different configurations are listed in Table 2. For each configuration, the CCD was exposed to x-rays from most of the 12 avaliable targets. For each target, a sequence of exposures was taken with about 4 to 5 different x-ray fluxes generated by using different tube currents (the tube voltage was held constant at 15 kV). The range of fluxes covered an approximately even spread up to twice the nominal flux used during the ACIS calibration.

Table 2. Pileup measurement configurations.

CCD	Date	Electronics	Exposure Time	Comments
w103c4	03jun96	Lbox	7.22	Early HEXS configuration
w103c4	16jan97	Lbox	7.22	
w103c4	12feb97	Lbox	7.22	
w140c4r	22jan97	DEA	3.28	Back sided CCD
w163c3	27sep96	DEA	3.28	
w190c3	26nov96	DEA	3.28	
w203c2	07may97	DEA	3.28	
w203c2	08may97	DEA	7.15	Lbox exposure time
w203c4r	16jan97	DEA	3.28	
w210c3r	12may97	DEA	3.28	
w210c3r	12may97	DEA	7.15	Lbox exposure time

An important assumption for the process is that the x-ray flux from HEXS varies linearly with the x-ray tube current. This was checked two different ways. First, the actual tube current was measurered using three different current meters and compared to the front panel display. All agreed within error. Secondly, the total electron charge detected by the CCD was found to be linear with tube current. The total charge is a reliable quantity since is does not depend on any event selection criteria. This data is presented in the next paragraph.

An example of the data products for w203c2 with a 7 second exposure are shown in Figs. 4 - 7. The left hand column plots the number of detected counts in the K_α per frame per quadrant and normalized to the x-ray tube current (in units of μA), versus the x-ray tube current. The counts are determined by fitting a three parameter gaussian curve to the K_α peak and using the fitted coefficients to determine the total counts. The four grade selections displayed are G0 (triangles), G0234 (stars), G02346 (squares), and G01234567 = All (diamonds). The value for each quadrant is plotted independently. The lines result from a least squares polynomial fit to Eq. 5. The fit for each quadrant is plotted independently. The zero current intercept averaged for all four quadrants is listed in the first column within each figure, and the zero current slope is listed in the second column. The third column is the slope normalized by the square of the intercept and multiplied by 10^5, which is called the rate. This number provides a configuration-independent slope which only depends on the number of detected x-rays, not on the x-ray tube current. The units for the rate are $(\mathrm{Counts/Frame/Qd})^{-1}$. The fourth column displays the error for the rate.

If there was no pileup horizontal lines would result. The non-zero slope of all the lines clearly indicates the presence of pileup. The presence of a non-linear slope for high Z indicates higher order pileup events, for which the quadratric correction of Eqn. 5 becomes important.

In the righthand column are similar plots for the number of pixels above the threshold (diamonds) and the total charge collected (triangles). Printed underneath the values of intercept and slope are the respective errors. The fact that the normalized charge doesn't vary significantly with x-ray tube current is good evidence for linearity of the x-ray flux with tube current.

Figures 8 and 9 are parallel figures for Figs. 4 -7, except the analysis uses all x-rays in the spectrum, not just those in the K_α peak. A useful number in these plots is the intercept for x-rays of all grades from which no-pileup branching ratios can be computed.

For our pileup analysis, the most significant number presented in each figure is the rate and error for the G02346 grade set, the set used most commonly for the ACIS calibration. These figures were produced for all 11 test configurations, although the other 10 configuration's figures are not included for space reasons. A summary for the G02346 rate values for all configurations is presented in Figs. 10 and 11. Figure 10 shows the rate for the first six elements. The graph for each element shows the rate value with errors for each test configuration. Not every configuration has a value for every element since due to some experimental problems and time constraints. A mean value has been determined for the front sided data (i.e. not including w140c4r), excluding any suspicious data points. The mean value is plotted as the horizontal dashed line and is printed in the upper right of each figure. Figure 11 corresponds to Fig. 10, except for the next six elements.

Figure 12 presents a summary of the mean rate values, both as a function of the K_α energy (top) and the x-ray penetration length (bottom) in silicon. With the exception of the Cl line at 2621 eV, the rate si roughly a constant at low energies, and increases quickly at high energies. The Cl line is a known exception since the target source is actually KCl and the K line competes with the Cl, causing more relative pileup than the other targets.

An example of pileup corrections for an ACIS CCD is shown in Table 3. Typical detected flux rates for the CCD w215c4r (which presently is located in the I3 position of the ACIS flight focal plane) are listed in the second column for the 13 different K_α x-rays listed in the first column (Mn K_α has now been included, whose source is radioactive Fe^{55}). The third column lists the mean values for $\hat{\epsilon}$ presented in Figs. 10 and 11. The fourth column are the corresponding incident fluxs as determined by Eqn. 6, and the next column is ratio N_i/N_d. These measurements were conducted with a 3.28 s exposure time. The last column lists the corresponding ratio if a 7.15 second exposure time had been used for the same incident flux.

Table 3. Example of pileup correction factors for typical detection fluxes in w215c4r

K_α X-ray	Detected Flux	$\hat{\epsilon}$	Incident Flux	Correction Factor	Correction Factor
	(G02346)	(10^5)	(G02346)	(3.28 sec)	(7.15 sec)
Al	1145	6.69	1245	1.086	
Si	1310	4.88	1403	1.071	1.161
P	1120	7.15	1222	1.091	1.210
Cl	605	11.1	650	1.075	
Ti	1285	4.62	1369	1.065	1.148
V	1180	4.57	1249	1.059	
Mn	1040	7	1140	1.096	1.190
Fe	950	8.07	1060	1.115	
Co	840	10.3	956	1.138	
Ni	700	13.5	811	1.159	
Cu	660	18.2	819	1.241	1.384
Zn	490	26.4	671	1.370	
Ge	880	46.9	940	1.068	

4 Spectral Correction Factors

The previous analysis is directly linked to the spectra emitted by HEXS. That is, $\hat{\epsilon}$(E) include effects of spectral impurities. For a more general analysis we desire to compute ϵ, which is independent of the spectra. Equation 4 gives the relation between $\hat{\epsilon}$ and ϵ in terms of α (the fraction of bad events per good event) and ϵ (xxx) (the average ϵ associated with the rest of the spectrum). Mathematically, a direct solution for ϵ(E) from the 12 different energies is complicated and we use an interative approximation. Using the numbers tabulated in Figs. 4 - 9, we compute α for each data set, with the results presented in Figs. 13 and 14. Using the results of Fig. 10 and 11, the average value $\epsilon^{'}$ for the rest of the spectrum is computed. Together with α, new values of $\epsilon^{'}$ are generated according to Eqn. 5, and the process is repeated until the values stabilize. Figures 15 and 16 show the average value of $\epsilon^{'}$ for the rest of the spectrum for all 12 energies. Finally, Figs. 17 and 18 are the computed values of ϵ, which are summarized in Fig. 19. Figure 19 represents the main result of this work, that is, the pileup crossections versus energy for a monochromatic beam. Notice that the low energy values are close to the theoretical minimun discussed above, 3.4×10^{-5}, corresponding to an area of 9 pixels in one CCD quadrant.

5 Branching ratio variation with flux

6 Applications to continuum spectra

7 Single Pixel Pileup

Pileup in a single pixel with a monochromatic source is easily understood as a simple poisson process. That is, if the probability for an x-ray to interact with a pixel during one exposure is μ, then the probability that N x-rays interact during one exposure is

$P_N = \frac{\lambda^N e^{-\lambda}}{n!}$

Consider an observation of N_{frame} exposures. If there was no pilup, the total incident flux of $N_i = N_F\lambda$ x-rays would be detected. The effect of pileup is that several or many x-rays may add during one exposure. Let

$N_0 = N_F e^{-\lambda} \equiv$ number of frames with no interaction.

Combining these two equations yields,

$\frac{N_i}{N_{frame}} = -log(\frac{N_0}{N_{frame}})$

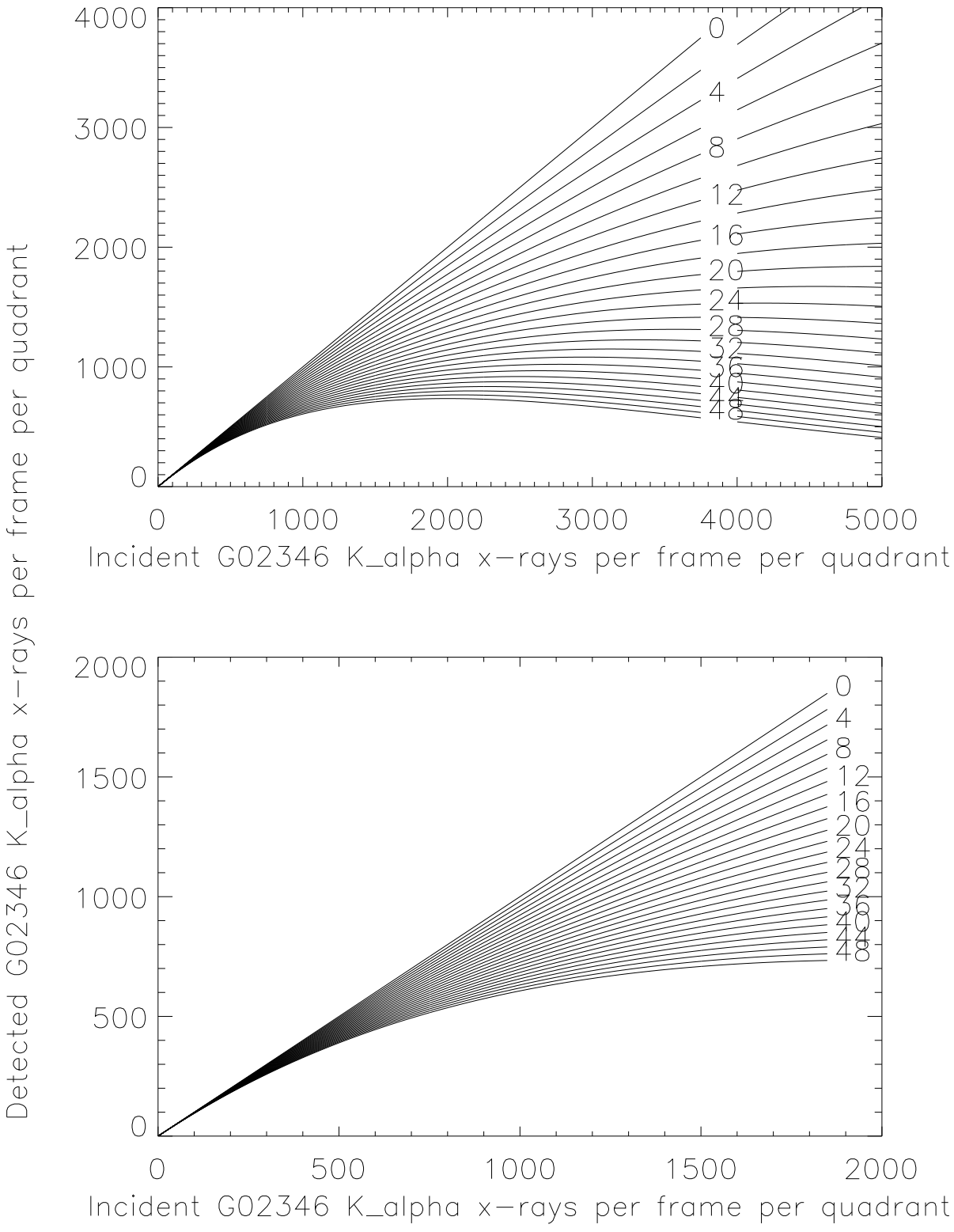

Figure 3: Relation of detected events to incident events accoring to Eqn.6

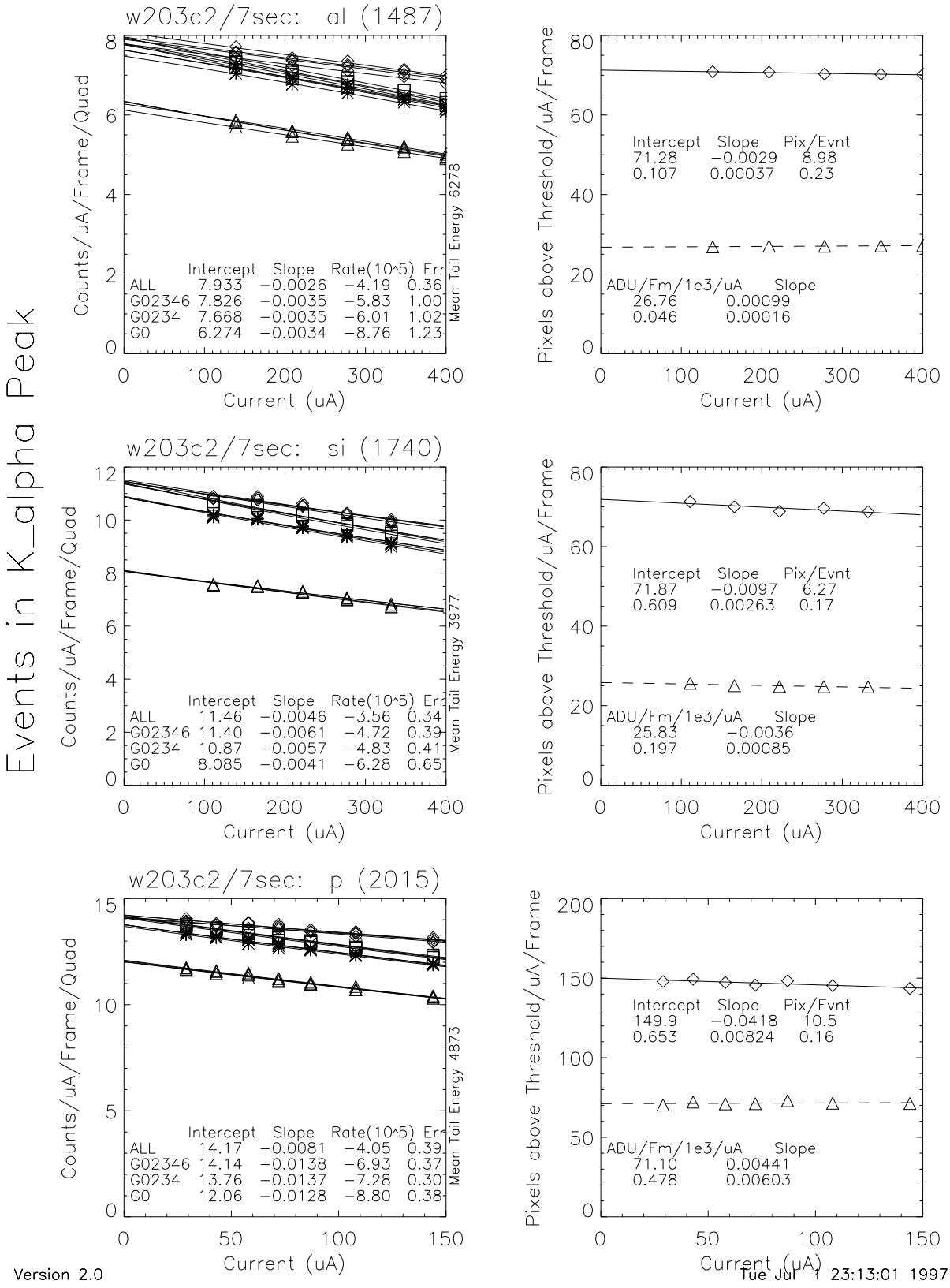

Figure 4: Raw HEXS pileup data for K_α for w203c2 with a 7 second exposure for Al,Si, and P targets

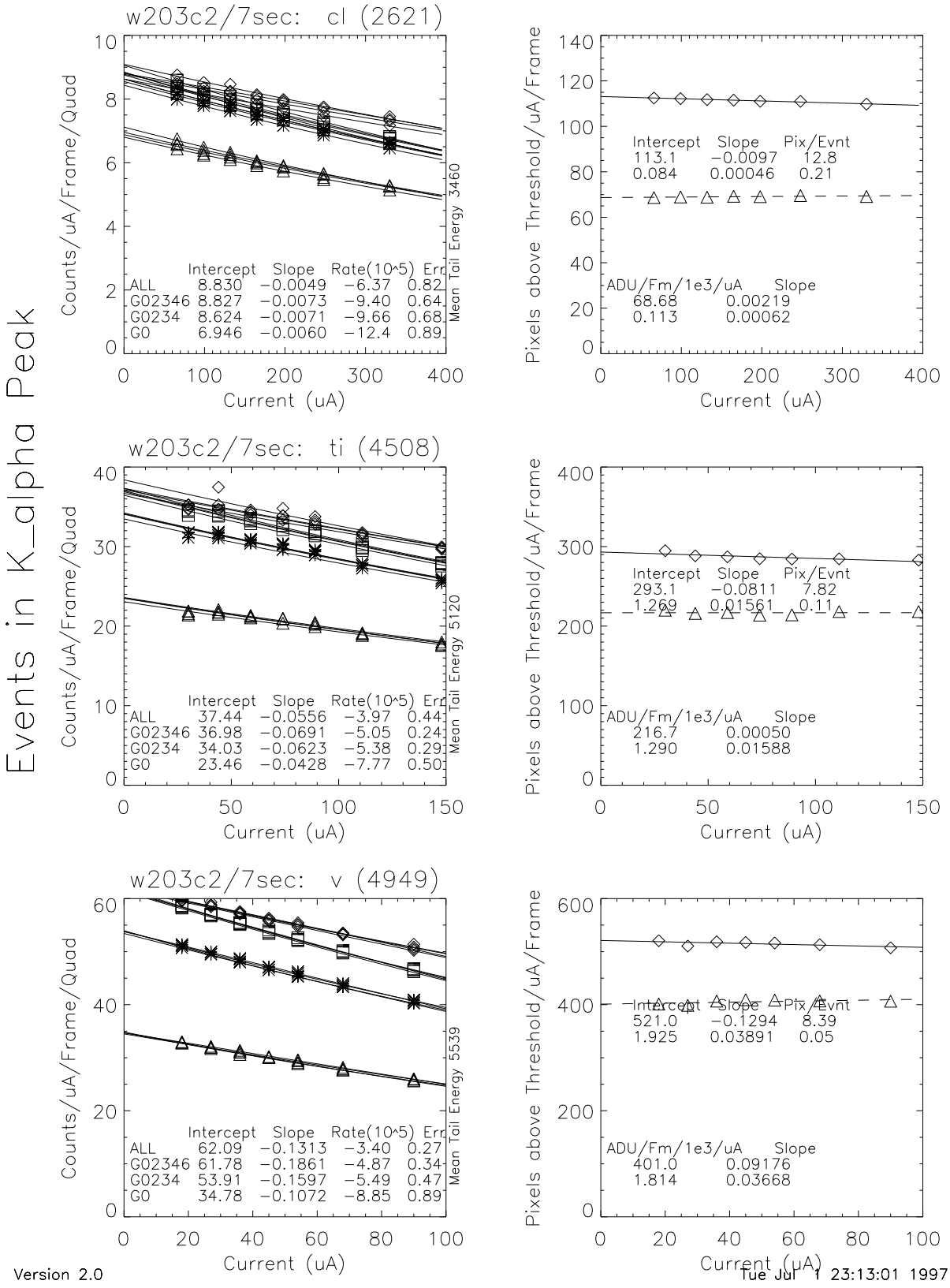

Figure 5: Raw HEXS pileup data for K_α for w203c2 with a 7 second exposure for Cl,Ti, and V targets

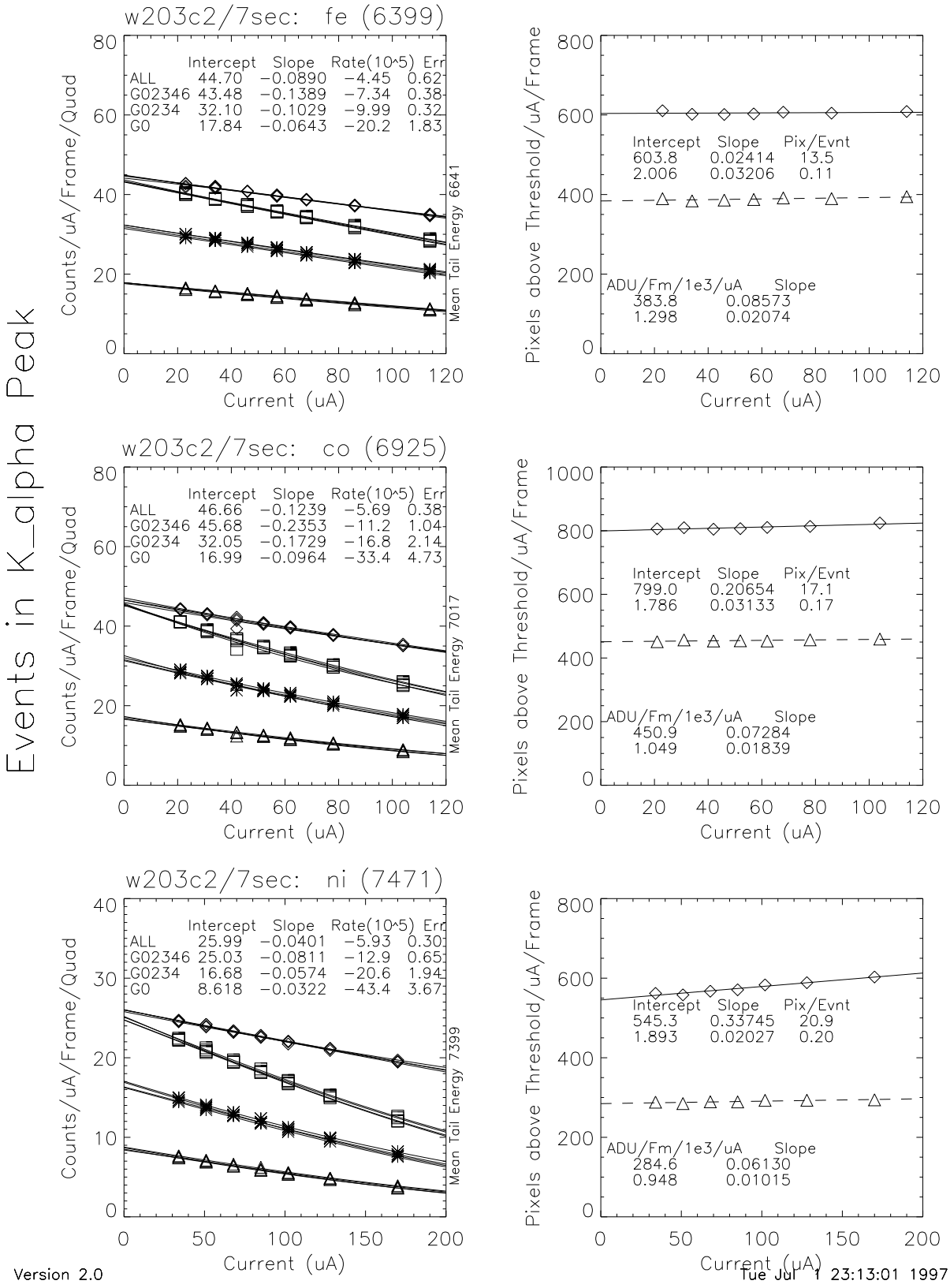

Figure 6: Raw HEXS pileup data for K_α for w203c2 with a 7 second exposure for Fe,Co, and Ni targets

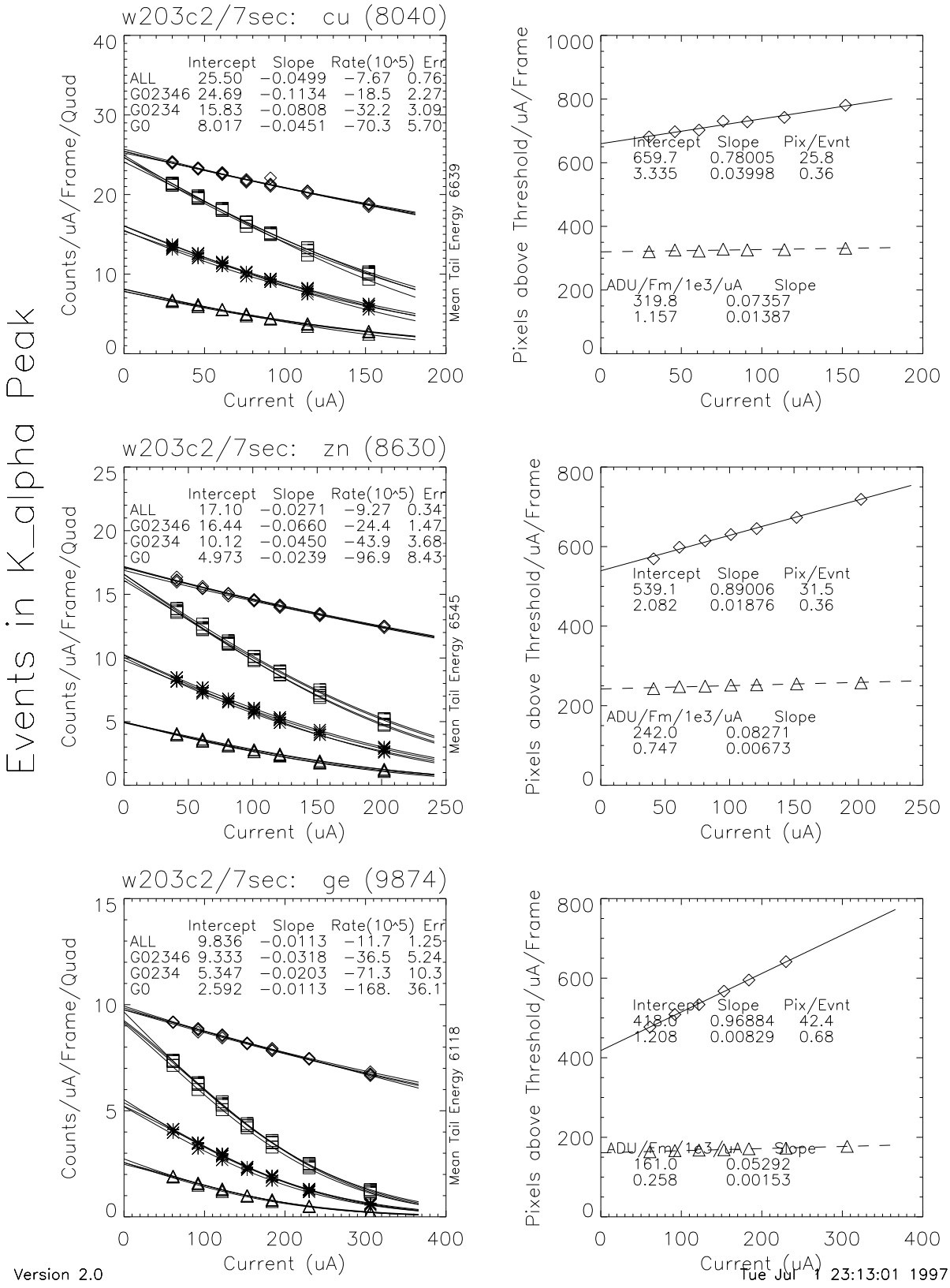

Figure 7: Raw HEXS pileup data for K_α for w203c2 with a 7 second exposure for Cu ,Zn, and Ge targets

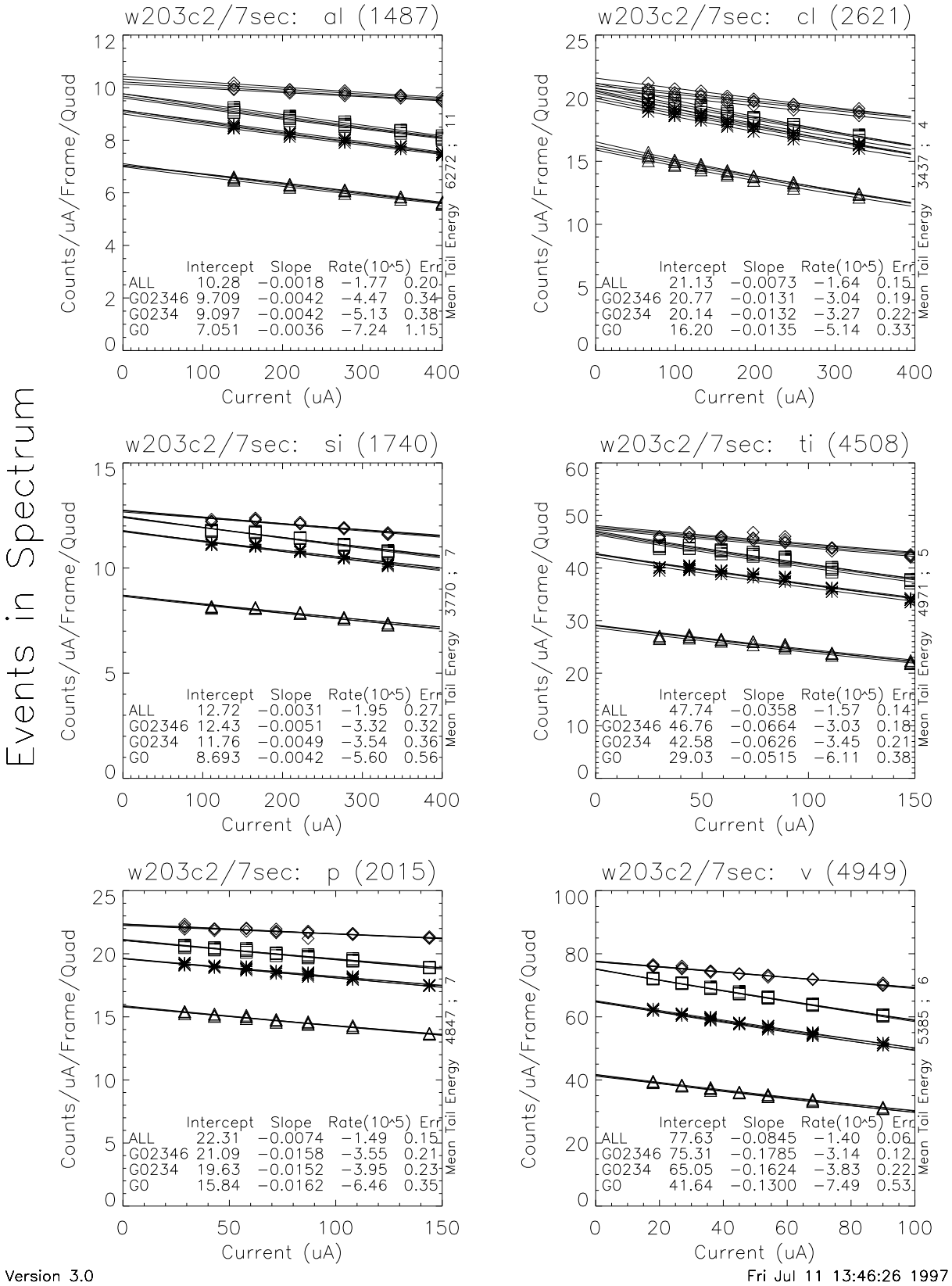

Figure 8: Raw HEXS pileup data for entire spectrum for w203c2 with a 7 second exposure for Al, Si, P, Cl,Ti, and V targets

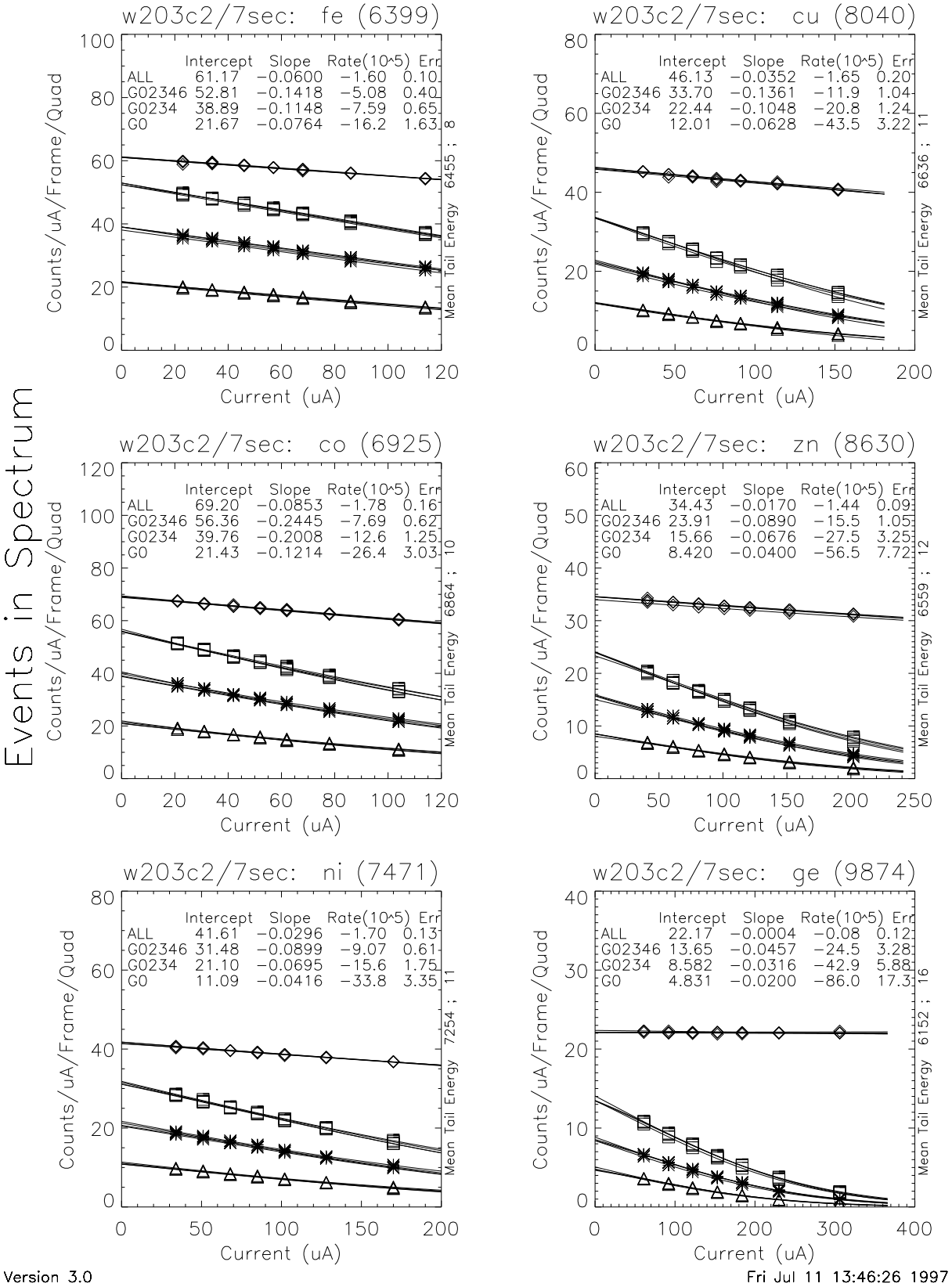

Figure 9: Raw HEXS pileup data for entire spectrum for w203c2 with a 7 second exposure for Fe, Co, Ni, Cu, Zn, and Ge targets

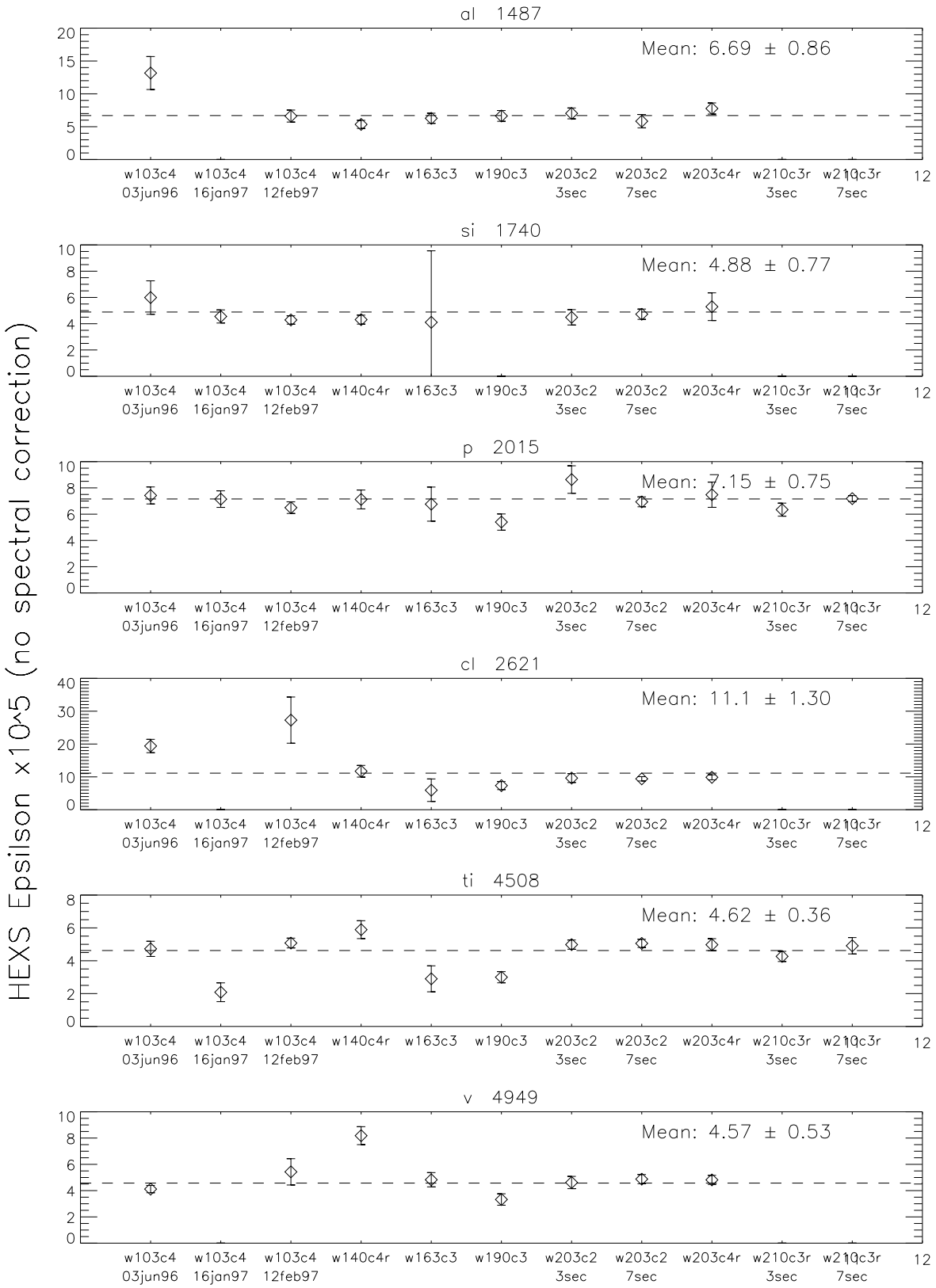

Figure 10: Mean g02346 epsilon for all data sets with no spectral correction (Al - V)

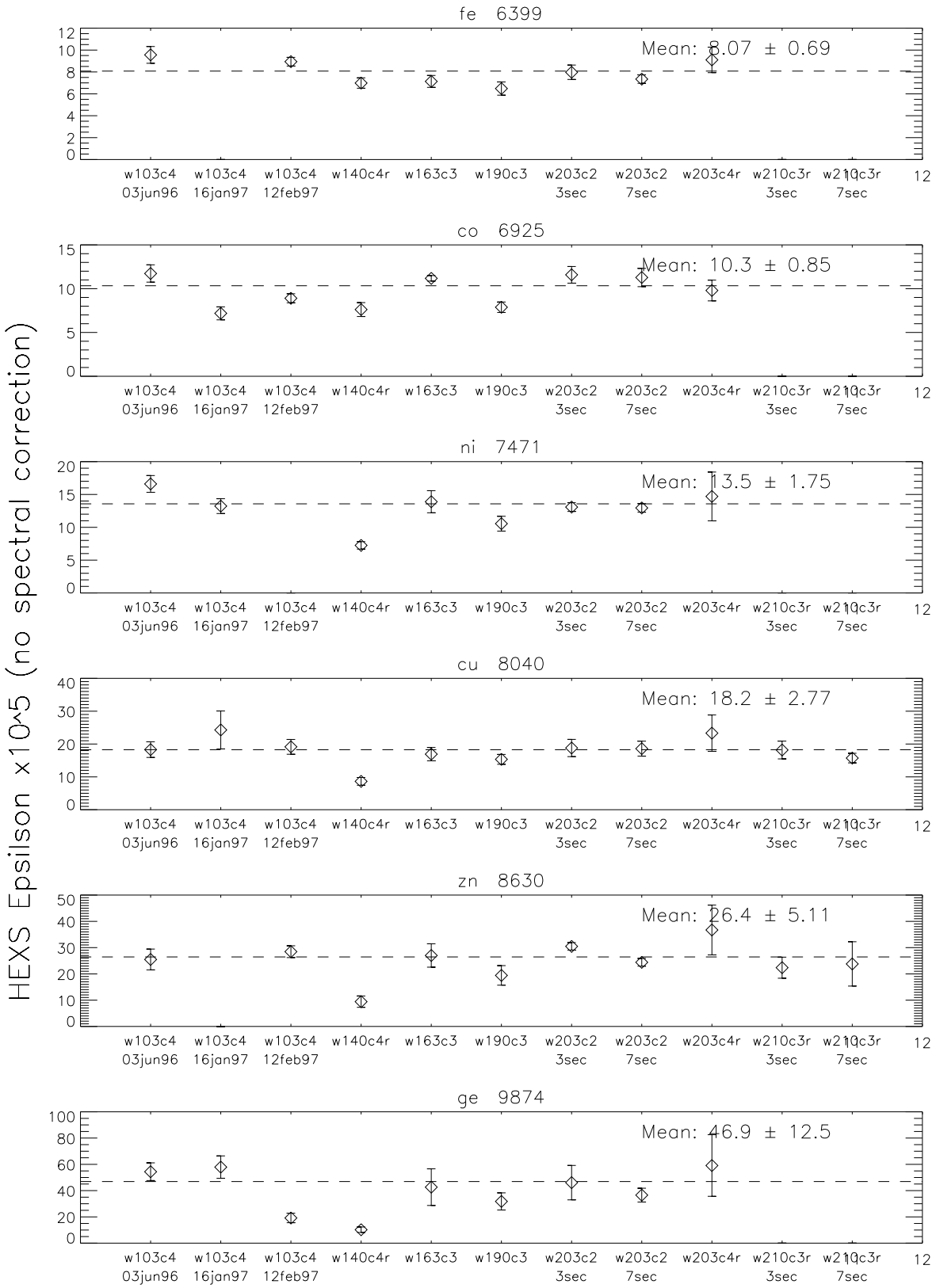

Figure 11: Mean g02346 epsilon for all data sets with no spectral correction (Fe - Ge)

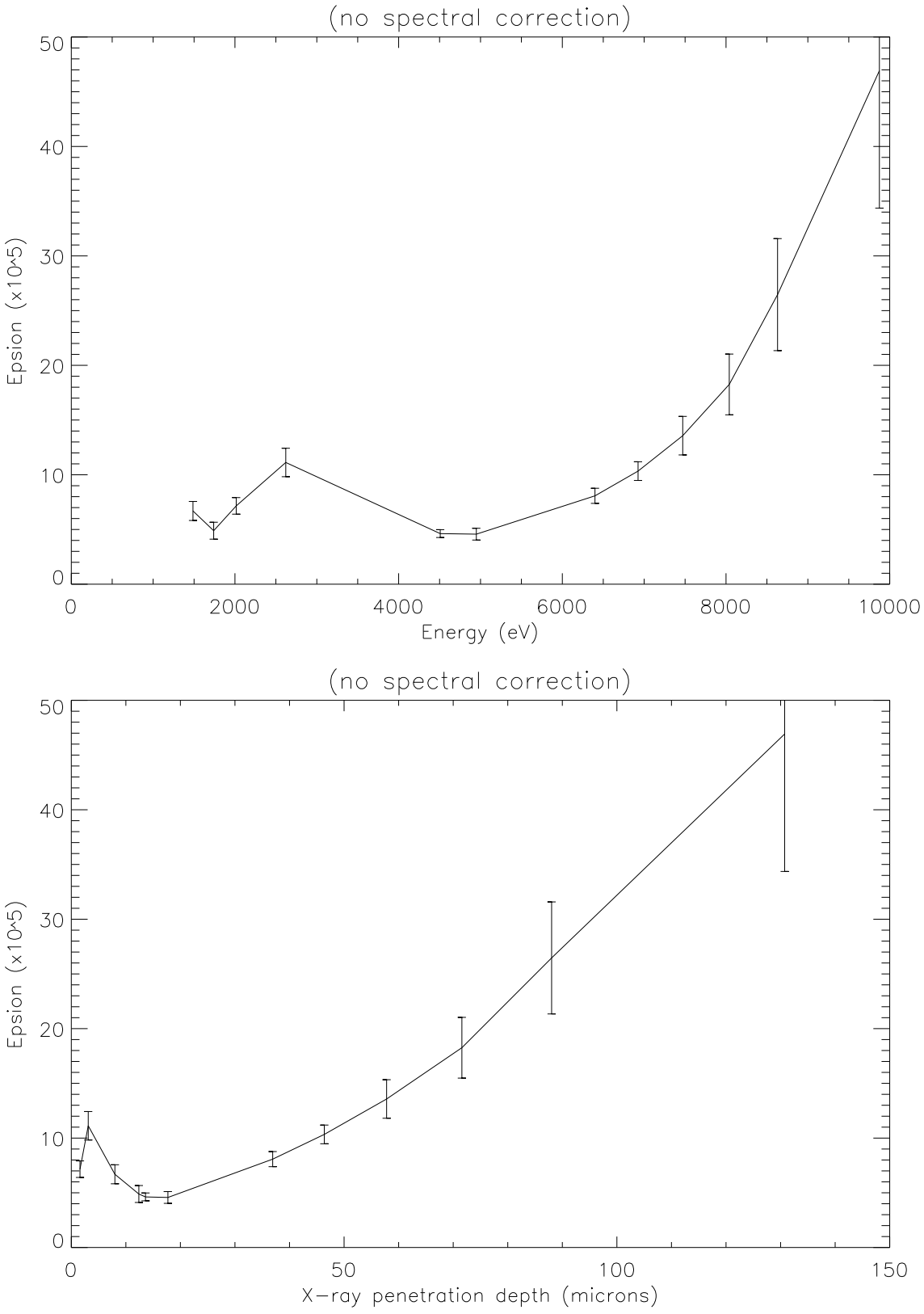

Figure 12: Variation of epsilon with for raw HEXS data

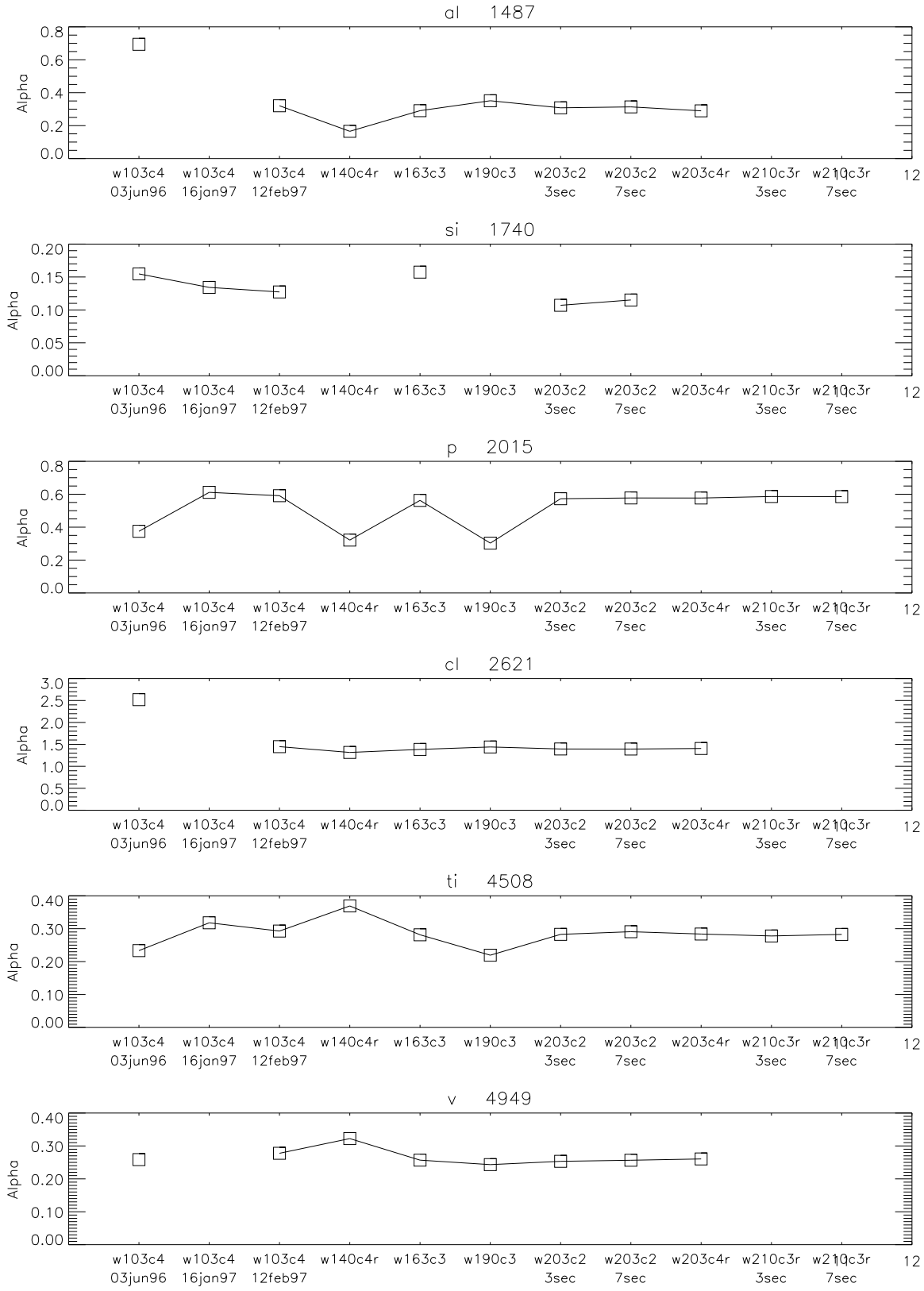

Figure 13: Variation of alpha, the ratio of bad to good x-rays, for Al to V

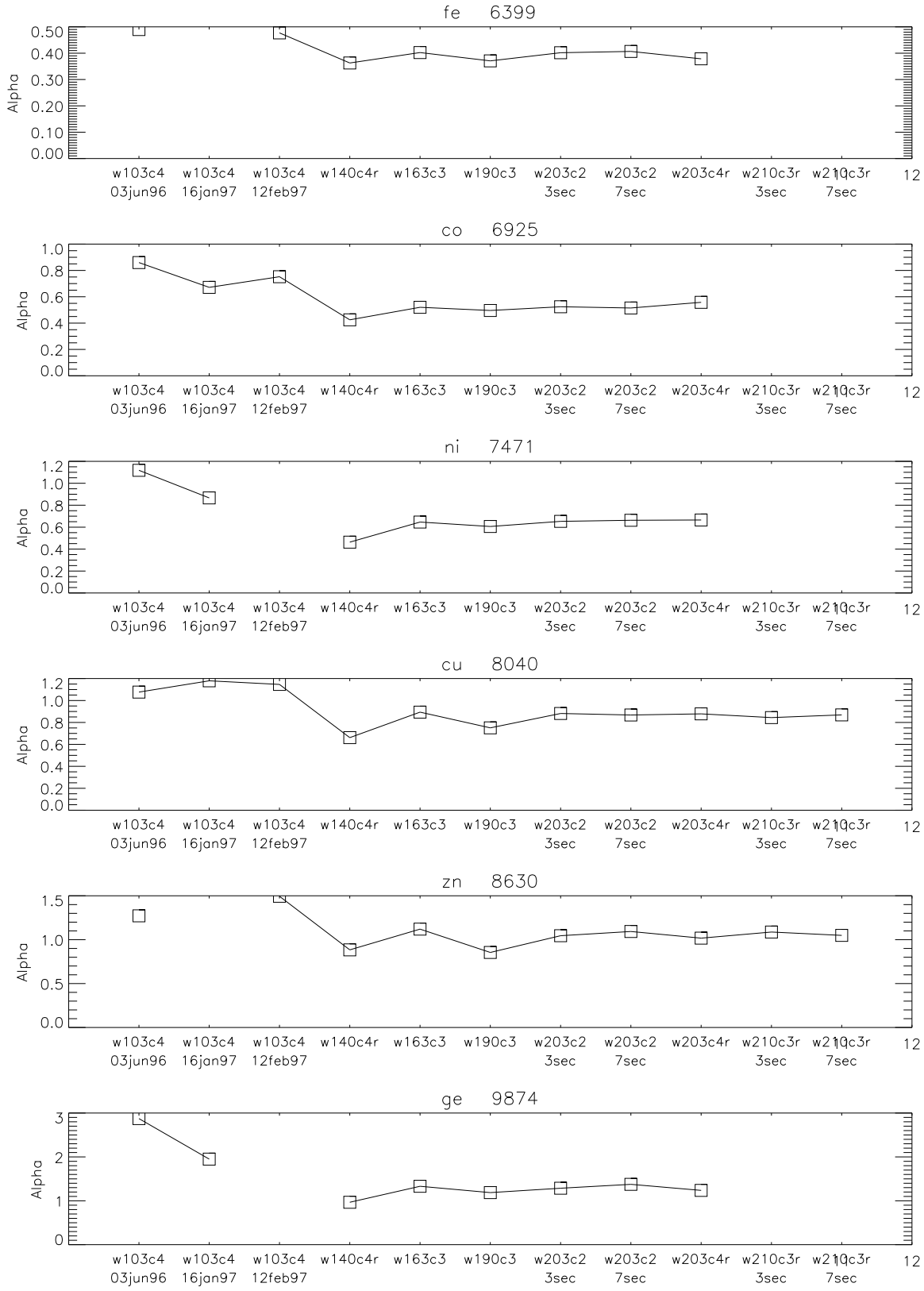

Figure 14: Variation of alpha, the ratio of bad to good x-rays for Fe to Ge

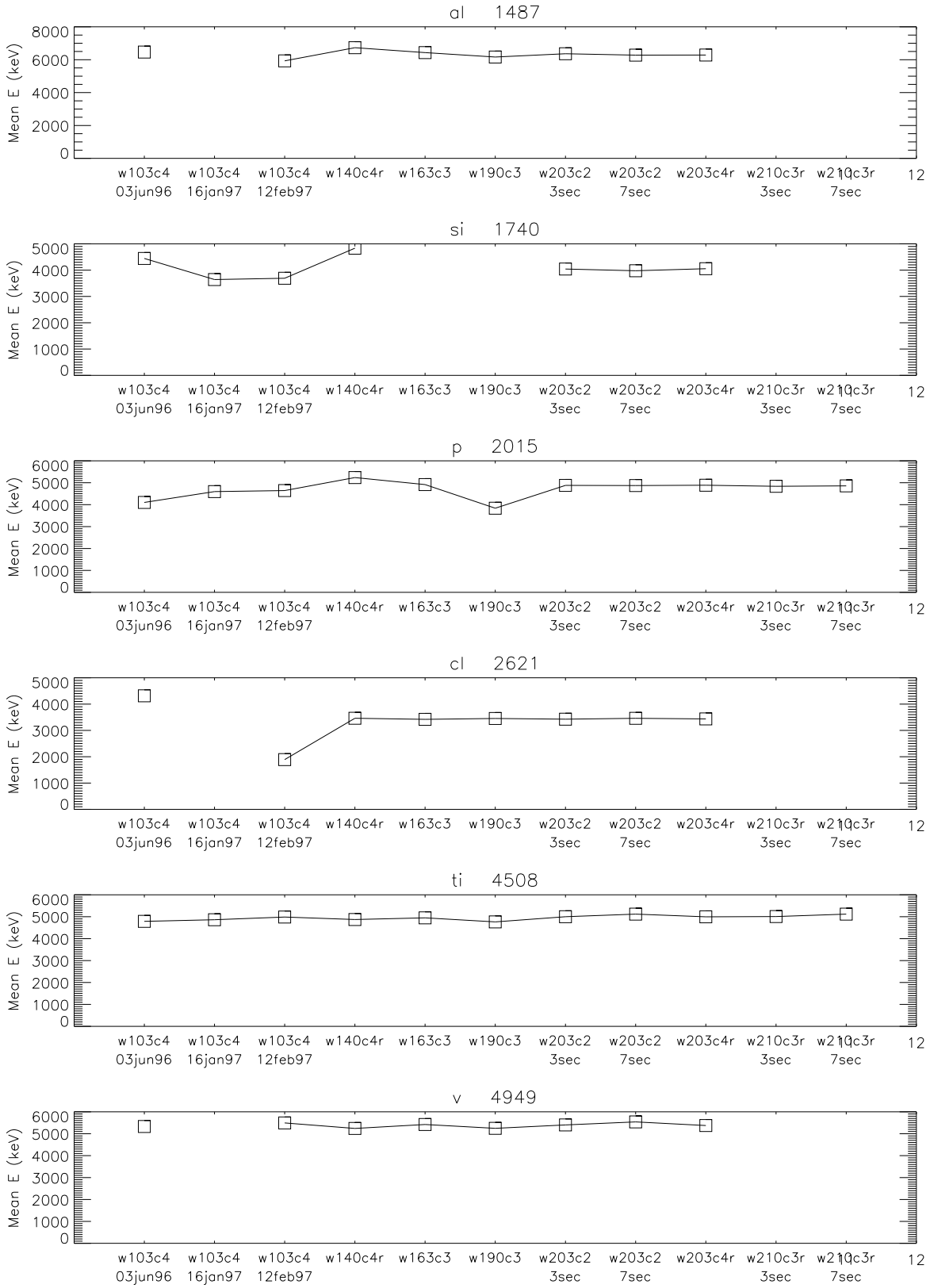

Figure 15: Variation of mean tail energy for Al to V

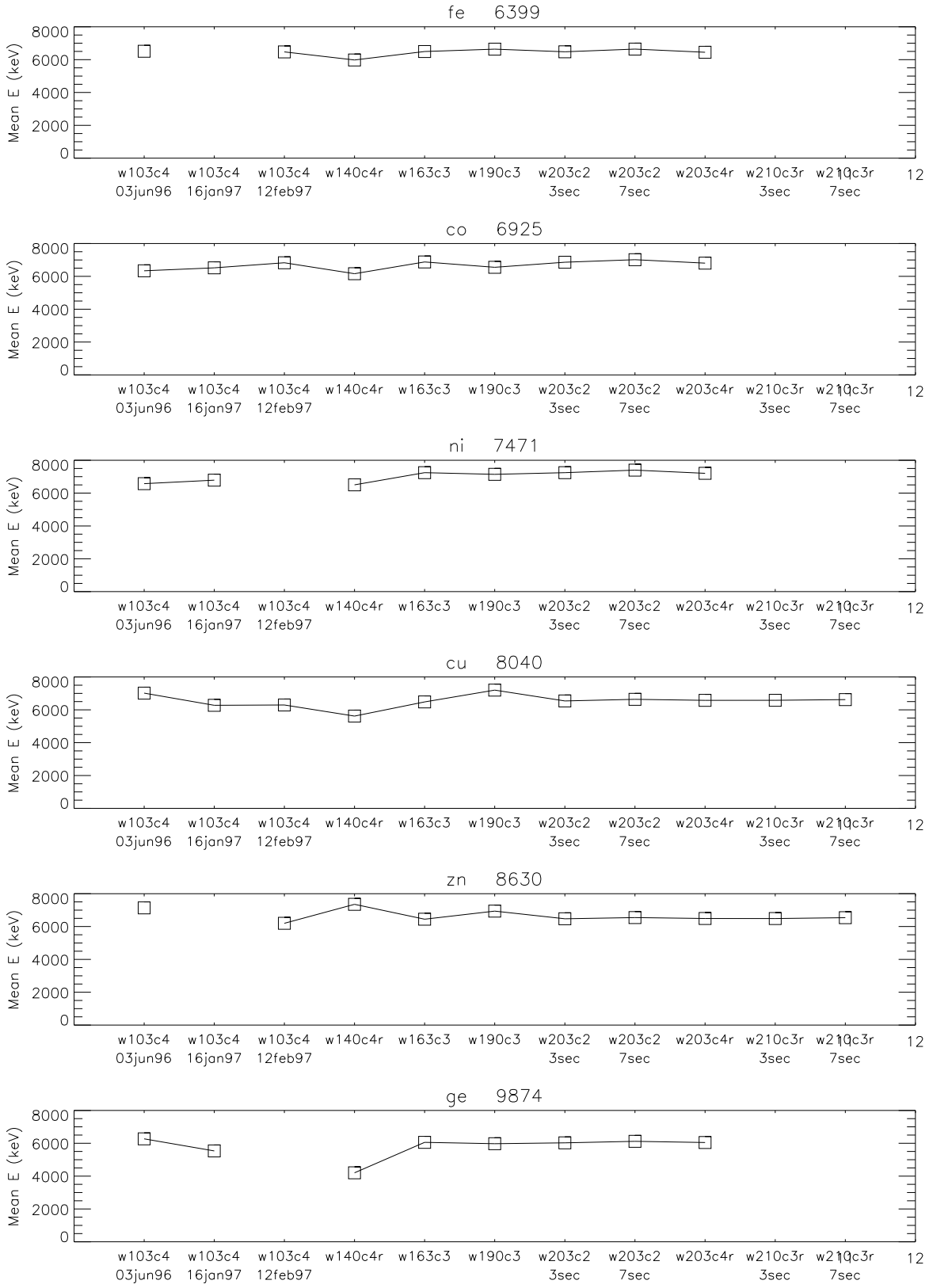

Figure 16: Variation of mean tail energy for Fe to Ge

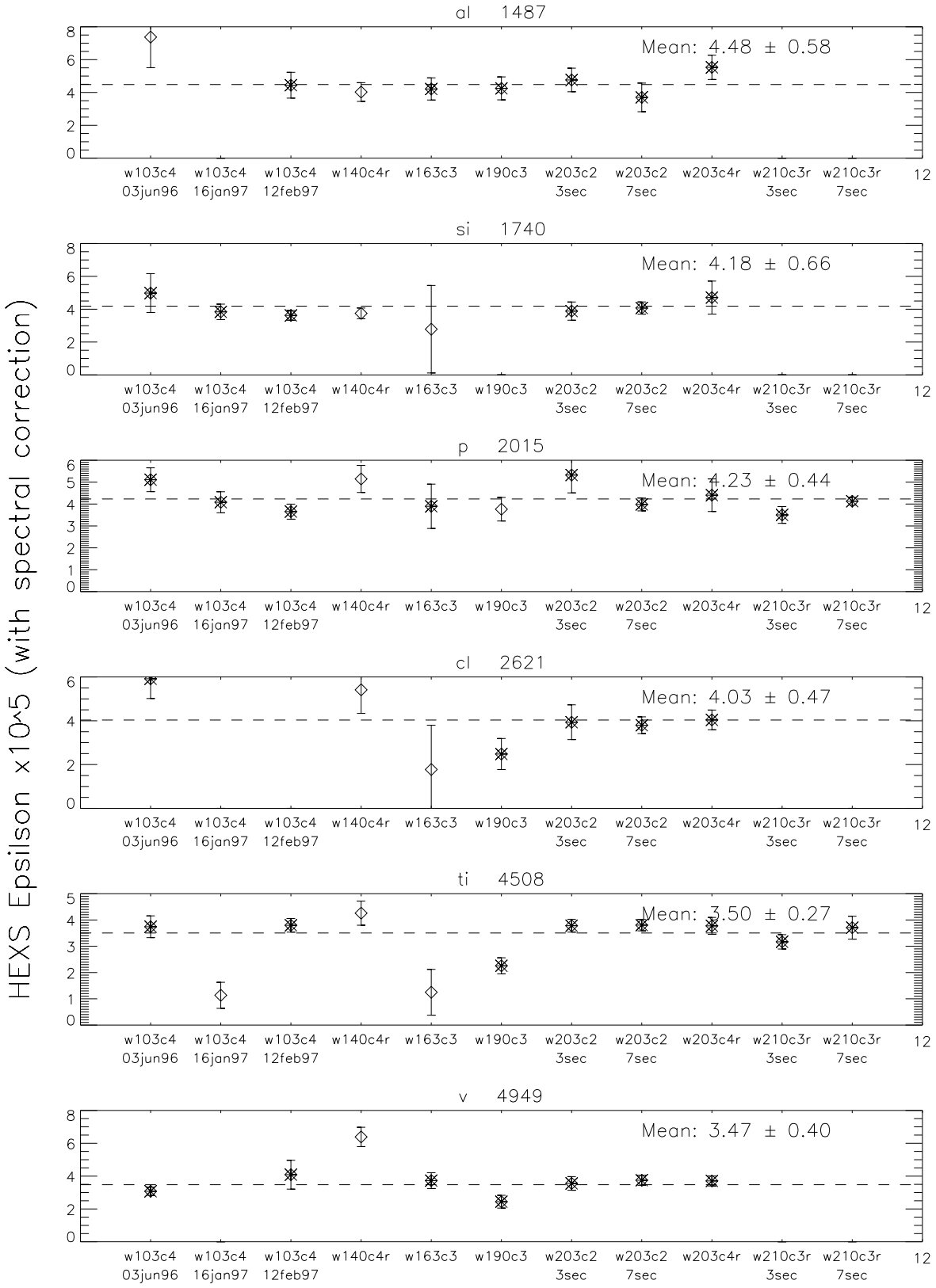

Figure 17: Mean g02346 epsilon for all data sets with no spectral correction

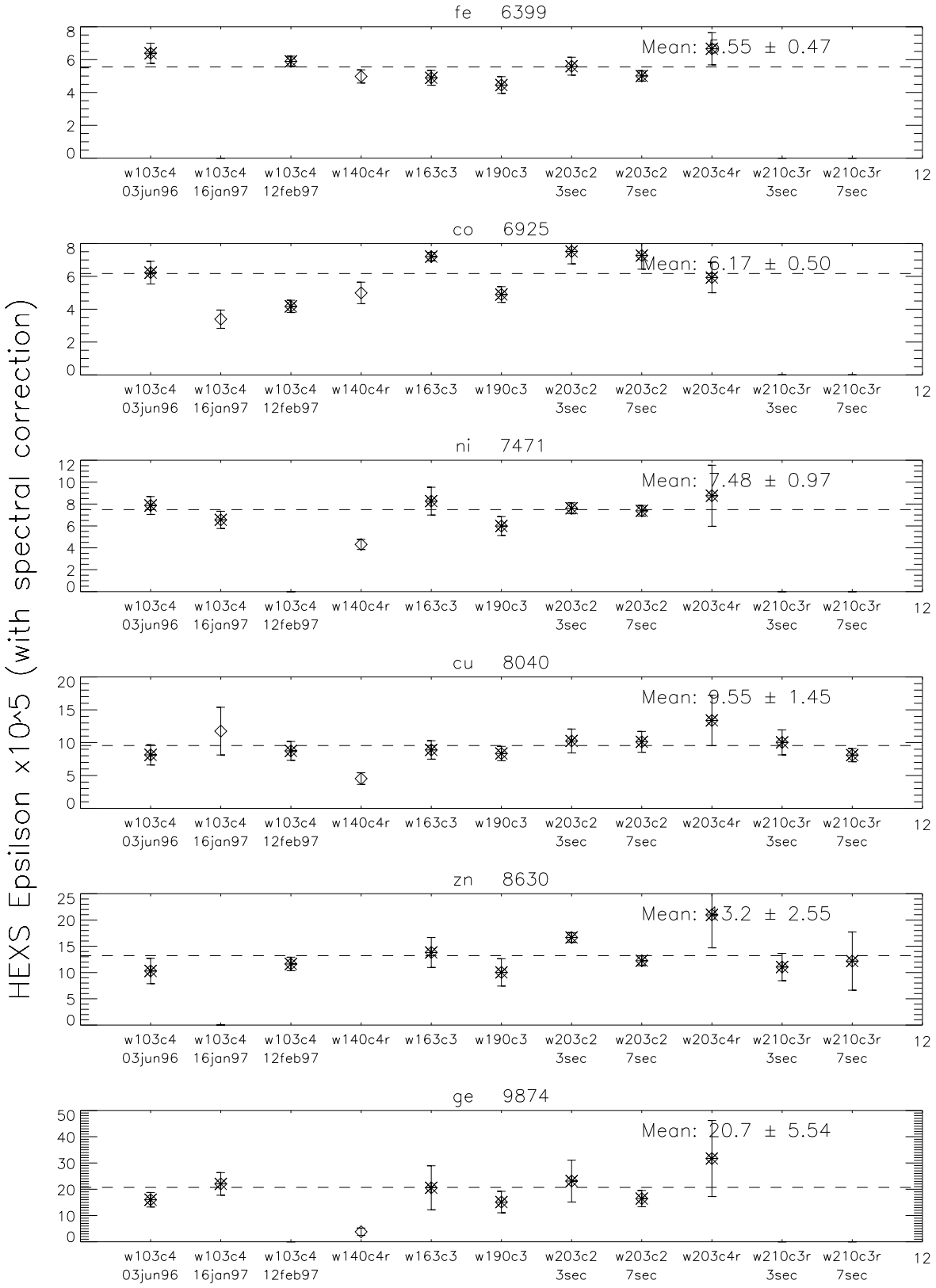

Figure 18: Mean g02346 epsilon for all data sets with no spectral correction

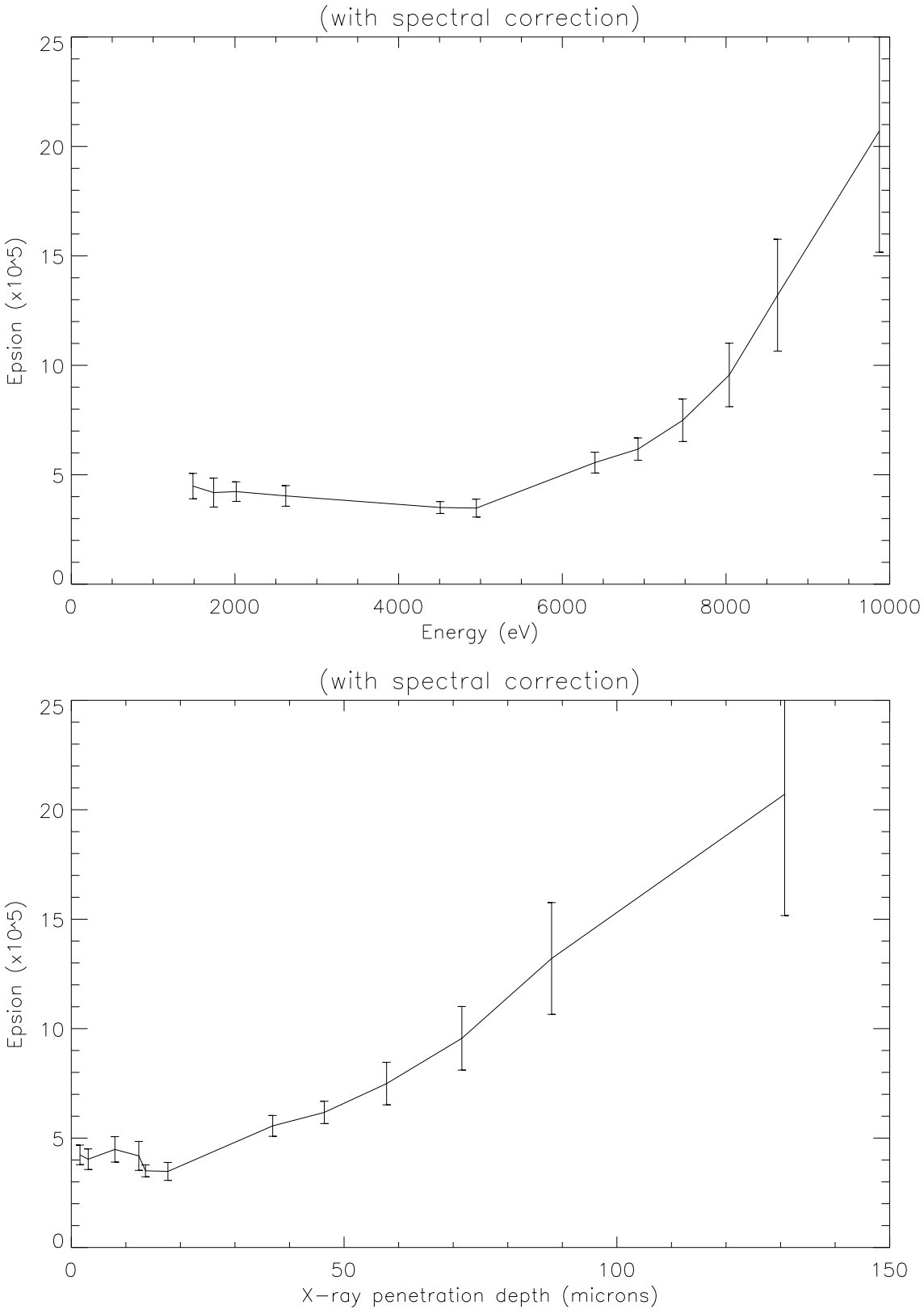

Figure 19: Variation of epsilon including corrections for spectral impurities

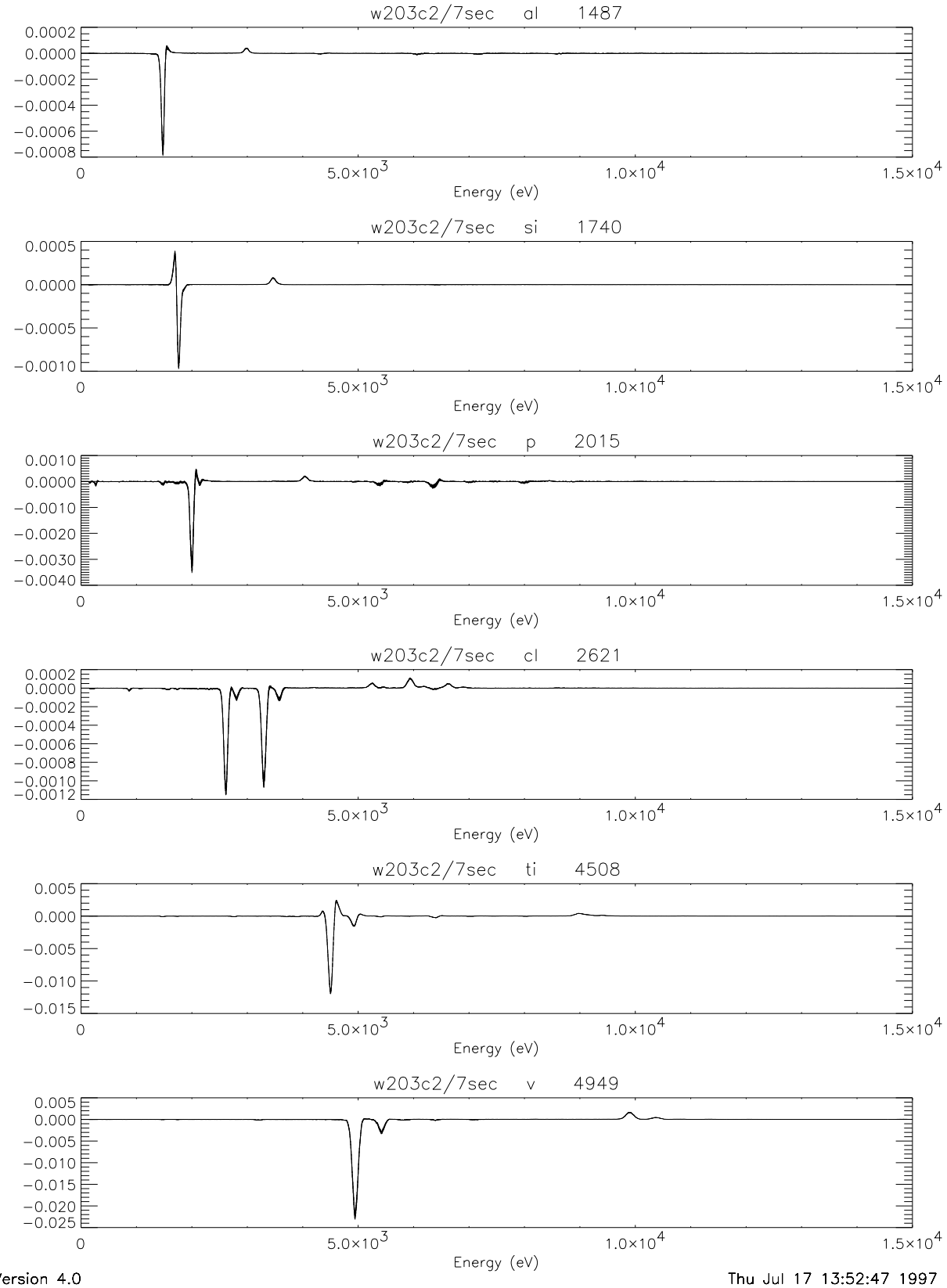

Figure 20: Redistribution of G02346 events in w203c2 during 7 second exposures due to pileup for Al, Si, P, Cl, Ti, and V HEXS targets